The Structure of TiO_2-SiO_2 Sol−Gel Glasses from Neutron Diffraction with Isotopic Substitution of Titanium and ^{17}O and ^{49}Ti Solid-State NMR with Isotopic Enrichment

David M. Pickup,* Frank E. Sowrey, and Robert J. Newport

School of Physical Sciences, University of Kent, Canterbury, CT2 7NR, United Kingdom

Philips N. Gunawidjaja, Kieran O. Drake, and Mark E. Smith

Department of Physics, University of Warwick, Coventry, CV4 7AL, United Kingdom

Received: March 2, 2004

Neutron diffraction with ^{46}Ti and ^{48}Ti stable isotopes and isotope-enriched ^{17}O and ^{49}Ti MAS NMR have been used to characterize the structure of $(TiO_2)_x(SiO_2)_{1-x}$ sol−gel glass as a function of composition (x = 0.08, 0.18, and 0.41) and calcination temperature (T = 250, 500, and 750 °C). The results reveal the first direct observation of two Ti−O distances in a homogeneous $(TiO_2)_{0.18}(SiO_2)_{0.82}$ sol−gel derived glass. In the sample heat treated at 250 °C, the Ti occupies a distorted octahedral environment similar to that found in the mineral ramsayite with four Ti−O bond lengths of around 1.89 Å and two close to 2.11 Å. After heating to 750 °C, two shorter bond distances are observed: a short distance at 1.81 Å due to tetrahedrally coordinated Ti and a longer distance of 1.94 Å due to a minority species of octahedrally coordinated Ti. The $(TiO_2)_{0.08}(SiO_2)_{0.92}$ sample exhibits similar behavior. After heating to 250 °C, two Ti−O distances are observed at 1.84 and 2.10 Å consistent with the presence of both tetrahedral and distorted octahedral titanium. Heating to higher temperature (500 or 750 °C) leads to the presence of only a single Ti−O distance at 1.82 Å consistent with all the titanium being substituted in tetrahedral sites within the silica network. ^{17}O NMR on samples at 45 atom % isotopic enrichment is very sensitive to phase separation. The $(TiO_2)_{0.18}(SiO_2)_{0.82}$ sample exhibits only a very small amount of phase separation in the form of a weak but nevertheless definite Ti−O−Ti signal. More significant phase separation of TiO_2 can be observed in the ^{17}O NMR spectrum from the $(TiO_2)_{0.41}(SiO_2)_{0.59}$ sample after heating at both 250 and 500 °C. ^{49}Ti NMR spectra are quite broad in all samples but some trends in line width and position are discerned. The results presented here are consistent with, but greatly extend, previous XRD, ^{17}O and ^{29}Si MAS NMR, XANES, and EXAFS studies of these materials.

Introduction

Understanding why amorphous materials exhibit the properties they do is both an intrinsically interesting scientific problem and fundamental to the task of tailoring useful properties and designing better materials for the future. An essential step in achieving this understanding is gaining a full knowledge of the atomic scale structure of such materials. Titania−silica mixed oxide glasses, $(TiO_2)_x(SiO_2)_{1-x}$, have received much attention over recent years because their physical properties lend them to a number of technological uses. They have found use as ultralow thermal expansion glasses[1] and thin films with tailored refractive indices.[2] However, the majority of the recent work on the titania−silica system focuses on its catalytic properties,[3−5] and in particular on how these are related to the local environment of titanium in the structure.

There have been several structural studies on $(TiO_2)_x(SiO_2)_{1-x}$ sol−gel glasses focusing both on the titanium environment and on the degree of phase separation between the oxide components. Walther et al.[6] used ^{29}Si MAS NMR to demonstrate that a two-stage reaction involving partial hydrolysis of the Si precursor, tetraethyl orthosilicate (TEOS), is necessary to obtain a homogeneous product. Dirken et al.[7] used a combination of ^{17}O and ^{29}Si MAS NMR to confirm the need for a two-stage reaction to obtain homogeneous, atomically mixed samples and demonstrated that ^{17}O NMR is a powerful technique for observing phase separation in such systems. This study also revealed that phase separation occurs in gels with a high titanium content (∼41 mol %). Extended X-ray absorption fine structure (EXAFS) has been used to directly probe the titanium environment. Anderson et al.[8] used EXAFS to measure the Ti−O bond distance in gels containing 8, 18, and 41 mol % of Ti. The results indicated an increase in the average Ti−O bond distance from 1.8 to 1.9 Å with increasing titanium content from 8 to 41 mol %; this change was attributed to the titanium environment changing from substituted within the silica network to phase separated into domains of TiO_2. Rigden et al.[9] used neutron and X-ray diffraction to study a similar set of samples and, on the basis of a measured Ti−O bond distance of ∼1.8 Å, reached the conclusion that titanium predominantly substitutes for silicon within the glass network. Despite the value of this study, the limited resolution of the X-ray data and the problem with overlapping correlations in the pair distribution function obtained from the neutron data precluded a full analysis of the titanium site. One of the most useful techniques for studying titanium-containing oxides is XANES, which indirectly yields information on the titanium environment from the shape of the Ti K-edge X-ray absorption profile and can distinguish between tetrahedral and octahedral coordinated titanium (TiO_4 and TiO_6, respectively, herafter).[10] Mountjoy et al.[11] exploited this technique to confirm two important structural trends that occur in

* Address correspondence to this author. E-mail: dmp@kent.ac.uk.

10.1021/jp049053j CCC: $27.50
Published on Web 06/19/2004

$(TiO_2)_x(SiO_2)_{1-x}$ materials. First, as the composition is varied from $x = 0.08$ to 0.41 there is a corresponding increase in the number of TiO_6 sites. Second, a clear correlation was established between the abundance of TiO_4 sites and the temperature of the heat treatment used in the gel-to-glass processing. More recently, the XANES technique was taken further and applied to samples that were heated in situ to temperatures of up to 250 °C.[12,13] These studies both revealed the existence of TiO_6 sites which could be reversibly converted to TiO_4 sites upon heating to 150−250 °C.

Despite the many studies outlined above, the exact nature of the titanium site has never been fully characterized. Here, for the first time, we combine two advanced structural probes in the study of this class of material: neutron diffraction with isotopic substitution (NDIS) can provide unambiguous and quantitative information on the Ti environment, while ^{17}O MAS and ^{49}Ti static NMR can directly probe the local structure.

Neutron diffraction has been widely used to investigate the structure of melt-quenched silicate glasses[14] and there are a few examples where the technique has been applied to the structure of silica-based sol−gel derived glasses.[9,15,16] Diffraction methods give access to both short- and medium-range order (up to ∼15 Å). However, for multicomponent systems, the overlapping of coordination shells limits the structural information that can be extracted from the data. NDIS allows the separation of the partial pair distribution functions associated with one specific element in the sample.[17] With use of this technique, it is possible to fully characterize the coordination environment of the isotopically substituted element as well as determine its relationship to the glass network. Until now, there have been no NDIS studies on sol−gel prepared materials, probably due to the complexity of enriching the precursor reagents and the difficulty in preparing two sol−gel samples that do not differ significantly in structure or composition except for the isotopic substitution. This paper describes the first application of this technique to a sol−gel glass with use of the stable isotopes of titanium, ^{46}Ti and ^{48}Ti.

Solid-state NMR is an increasingly used atomic-scale, element-specific probe of the structure of materials.[18] ^{29}Si MAS NMR can determine the network connectivity by identification of the different Q^n species, and the loss of organic groups and hydroxyls can be followed by ^{13}C and ^{1}H NMR.[19] ^{17}O on enriched samples has been shown to be extremely sensitive to the distribution of the metals through identifying the different fragments (such as (Ti,Si)−O−(Si,Ti)) present,[7,19] and has been used to show differences in the degree of phase separation as the functionality of the silicon precursor was varied.[20] The maximum ^{17}O enrichment level used to date in such samples has been 20 atom %. Higher enrichment levels would be helpful to better detect the weaker signals from minority species; here, for the first time, results from such samples made with 45 atom % of ^{17}O-enriched H_2O are reported. $^{47,49}Ti$ have low natural abundance (5.51% for ^{49}Ti, 7.28% for ^{47}Ti) and small gyromagnetic ratios (γ).[18] These factors combine to produce relatively low intrinsic detection sensitivity, which is exacerbated for these titanium isotopes by the moderately large quadrupole moments. Titanium NMR has the additional difficulty that the two isotopes have almost identical γ values, so that even at 14.1 T the resonance frequencies differ by only ∼9 kHz. Given the typical widths of the resonances observed, most spectra will consist of completely overlapped resonances from the two isotopes.[18,21] There have only been a few reports of titanium NMR from amorphous materials.[22,23] To overcome these problems the samples studied here were enriched in ^{49}Ti and ^{48}Ti to 23.9 and 74.3 atom %, respectively; the latter enrichment had the effect of depleting the sample in ^{47}Ti. This approach greatly increases the signal and means that the NMR spectra may be regarded as arising effectively from the ^{49}Ti contribution alone.

The sample compositions used in this study have been chosen because they represent the full spectrum of behavior of TiO_2 in silica. The $(TiO_2)_{0.08}(SiO_2)_{0.92}$ and $(TiO_2)_{0.41}(SiO_2)_{0.59}$ sample are respectively well below and above the concentration range of 11 to 16 mol %, which is thought to be the limit of solubility of TiO_2 in sol−gel silica glass.[11,24] The $(TiO_2)_{0.18}(SiO_2)_{0.82}$ composition is particularly interesting because it is just above this limit of solubility and should therefore contain the maximum possible amount of titanium for silicon substitution.

Experimental Methods and Theory

Sample Preparation. Initially, samples of natural TiO_2, $^{46}TiO_2$ (72.1 atom % enriched, Isoflex USA), $^{48}TiO_2$ (99.8 atom % enriched, CK Gas Products), and $^{48/49}TiO_2$ (74.3 and 23.9 atom % enriched respectively, CK Gas Products and Isoflex USA) were converted to the corresponding isopropoxides via their chloride analogues. Each chloride was prepared by first grinding the oxide with an excess of carbon and heating (∼1000 °C) under a controlled atmosphere of chlorine in a fluidized-bed reaction vessel. The resultant $TiCl_4$ was condensed in a cold trap and purified by distillation.[25] The isopropoxide was prepared by reacting the $TiCl_4$ with anhydrous 2-propanol under a dry nitrogen atmosphere.[26] The HCl byproduct was converted to insoluble NH_4Cl by diluting the reaction mixture with anhydrous toluene (to reduce the solubility of the NH_4Cl) and bubbling through dry NH_3 for 2 h followed by heating at 60−70 °C for a further 2 h. The solid NH_4Cl was removed by filtration and the toluene boiled off under vacuum. The resultant $Ti(OPr^i)_4$ was purified by vacuum distillation.

The $(TiO_2)_x(SiO_2)_{1-x}$ ($x = 0.08$, 0.18, and 0.41) sol−gels were prepared by reacting the isotopically enriched $Ti(OPr^i)_4$ with TEOS (tetraethyl orthosilicate, $Si(OEt)_4$) in the presence of H_2O and HCl, using the procedure described previously.[27] In the case of the samples for the NMR study, 45 atom % of ^{17}O-enriched water was used. The samples were heated to 120 (NMR samples only), 250, 500, and 750 °C at a ramp-rate of 5 deg min^{-1} under an atmosphere of flowing air; each temperature was maintained for 2 h.

Isotopically enriched samples of the same composition were shown to be structurally equivalent by using X-ray diffraction (Station 9.1, Synchrotron Radiation Source, Daresbury Laboratory, UK). Further characterization necessary for analysis of the neutron diffraction data was performed: elemental analysis (ICP-AES and gravimetric) was carried out by a commercial company (Medac Ltd.) and macroscopic densities were determined by helium pycnometry. The results of this characterization are presented in Table 1.

Neutron Diffraction Theory and Method. The initial stage of analysis of neutron diffraction data from an amorphous material entails the removal of background scattering, correction for absorption and multiple scattering, and subtraction of the self-scattering term. The resultant scattered intensity, $i(Q)$, where $Q = 4\pi \sin(\theta/\lambda)$, can reveal structural information by Fourier transformation to obtain the total correlation function:[28]

$$T(r) = T^0(r) + \frac{2}{\pi}\int_0^\infty Qi(Q)\, M(Q) \sin(Qr)\, \mathrm{d}(Q) \qquad (1)$$

where $T^0(r) = 4\pi r\rho^0(\sum_i c_i b_i)^2$ is the average density contribution (ρ^0 is the macroscopic number density, and c_i and b_i are the

TABLE 1: Sample Characterization of Heat-Treated $(TiO_2)_x(SiO_2)_{1-x}$ Sol−Gel Glasses Containing Natural Titanium[a]

sample	composition (atom %) Ti	Si	O	C	H	$c_{Ti}/(c_{Ti}+c_{Si})$	density (g cm^{-3})
$x = 0.08$; 250 °C	1.6	17.9	54.9	3.1	22.5	0.08	2.10(5)
$x = 0.18$; 250 °C	3.4	16.1	56.3	2.9	21.4	0.17	2.23(5)
$x = 0.41$; 250 °C	8.8	13.4	58.9	0.8	18.2	0.40	2.35(5)
$x = 0.08$; 500 °C	1.9	23.4	65.4	0.00	9.3	0.08	2.18(2)
$x = 0.18$; 500 °C	4.4	20.7	62.9	0.00	12.1	0.17	2.27(2)
$x = 0.41$; 500 °C	10.8	16.4	65.6	0.00	7.3	0.40	2.61(2)
$x = 0.08$; 750 °C	2.0	23.7	61.0	0.00	13.3	0.08	2.25(2)
$x = 0.18$; 750 °C	4.4	21.4	61.3	0.00	12.9	0.17	2.36(2)

[a] c_x represents the concentration of atom type x.

atomic fraction and coherent scattering length, respectively, of element i), and $M(Q)$ is a modification function used to take into account the maximum experimentally attainable value of Q.

If two experiments are performed in which the scattering length of element A is varied (by isotopic substitution), the difference between the experimental correlation functions is of the form[29]

$$\Delta T(r) = T(r) - T'(r) = c_A{}^2(b_A{}^2 - b_{A'}{}^2)t'_{AA}(r) + 2\sum_{j\neq A} c_A c_j b_j (b_A - b_{A'})t'_{Aj}(r) \quad (2)$$

where $t'_{AX}(r)$ represents the partial pair correlation function for elements A and X. Thus, only the structural environment of element A is probed.

Structural information can be obtained from the neutron diffraction data by modeling the Q-space data and converting the results to r-space by Fourier transformation to allow comparison with the experimentally determined correlation function.[14] The Q-space simulation is generated by using the following equation:

$$p(Q)_{ij} = \frac{N_{ij} w_{ij}}{c_j} \frac{\sin(QR_{ij})}{QR_{ij}} \exp\left[\frac{-Q^2\sigma_{ij}{}^2}{2}\right] \quad (3)$$

where $p(Q)_{ij}$ is the pair function in reciprocal space, N_{ij}, R_{ij}, and σ_{ij} are the coordination number, atomic separation, and disorder parameter, respectively, of atom i with respect to j, c_j is the concentration of atom j, and w_{ij} is the weighting factor given by $w_{ij} = 2c_ic_jb_ib_j$ if $i \neq j$ or $w_{ij} = c_i{}^2b_i{}^2$ if $i = j$. The parameters N_{ij}, R_{ij}, and σ_{ij} are varied to obtain a satisfactory fit in r-space. In the case of the neutron difference experiment, the weighting factors used in the fitting process are slightly different: if $A \neq j$, $w_{Aj} = 2c_Ac_j(b_A - b'_A)b_j$ and if $A = j$, $w_{Aj} = c_A{}^2(b_A{}^2 - b'_A{}^2)$, where A again denotes the atom that has been isotopically substituted. In this case, A = Ti and, taking into account the degree of enrichment, the neutron scattering lengths are as follows: ^{46}Ti, $b = 2.469$ fm; ^{48}Ti, $b = -6.063$ fm; and ^{nat}Ti, $b = -3.438$ fm. It should be noted that the negative scattering lengths arise from a π phase shift of the neutron wave function on scattering.

The neutron diffraction data presented here were collected on the GEM diffractometer on the ISIS spallation neutron source at the Rutherford Appleton Laboratory, UK. The finely powdered samples were held in 6 mm diameter vanadium cans, which have a very low cross section for the coherent scattering of neutrons, and time-of-flight data collected over a wide range of Q (up to 50 Å^{-1}). The ATLAS suite of programs was used to reduce and correct the data.[28]

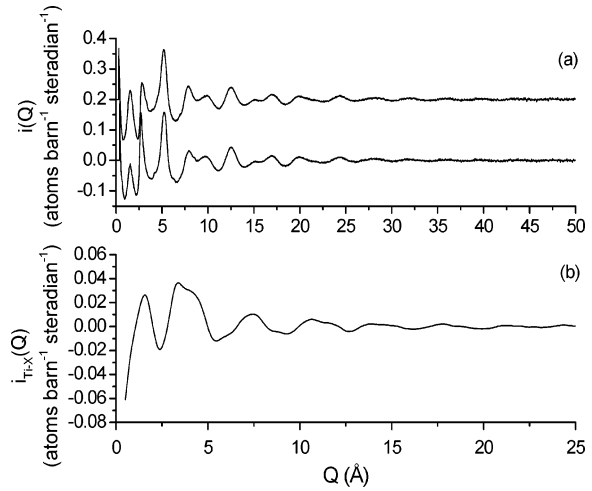

Figure 1. Typical Q-space neutron diffraction data from the isotopically enriched $(TiO_2)_x(SiO_2)_{1-x}$ sol−gel samples: (a) Q-space interference functions, $i(Q)$, from the ^{46}Ti-enriched (upper trace) and ^{48}Ti-enriched (lower trace) $(TiO_2)_{0.18}(SiO_2)_{0.82}$ samples heated to 750 °C and (b) difference interference function obtained by subtracting the ^{48}Ti $i(Q)$ from the ^{46}Ti $i(Q)$.

MAS NMR Methods. The ^{17}O MAS NMR spectra were collected with 4 mm MAS NMR probes (both Doty and Bruker) spinning at ∼12 kHz on a Varian Infinity CMX-360 spectrometer, equipped with an 8.45 T magnet, operating at 48.18 MHz. Spectra were collected with use of $\theta-\tau-2\theta$ spin−echo pulse sequences with θ corresponding to a tip angle of ∼90° on the solid sample (typically 1.5 μs), τ set to the rotor period, and recycle delays of 0.5−5 s, sufficient to allow relaxation. The number of co-added scans depended on the level of enrichment (and hence the heat treatment[19]) but was typically 3×10^4. Spectra were referenced to H_2O at 0 ppm. The ^{49}Ti NMR spectra were collected with use of a 9.5 mm Varian Chemagnetics T3 probe on at Varian CMX Infinity 600 spectrometer, equipped with a 14.1 T magnet, operating at 32.3 MHz. On static samples a spin−echo was used with a 90° pulse of ∼1.5 μs with a τ spacing of 50 μs and extended phase cycling.[30] A 0.1 s recycle delay was used, with 50k and 500k scans typically collected for the $x = 0.41$ and 0.08 samples, respectively. Spectra were referenced to the narrow resonances of cubic $SrTiO_3$ at 0 ppm, which occurs at −843 ppm with respect to the primary titanium shift reference of neat liquid $TiCl_4$.

Results and Discussion

Figures 1 and 2 serve to illustrate both the method and benefit of using NDIS to study this class of materials. Figure 1a shows the Q-space neutron diffraction interference functions for the isotopically enriched $(TiO_2)_{0.18}(SiO_2)_{0.82}$ sol−gel glasses heated to 750 °C. There are two points to note concerning these spectra. First, the data are of sufficient quality over a wide range of Q ($Q_{max} = 50$ Å^{-1}) to provide excellent real-space resolution when Fourier transformed. The second is to observe how similar the two spectra are. This is to be expected because the materials are mostly silica (over 80 mol %) and were prepared to be structurally equivalent: i.e. identical in all pertinent respects except for the isotope of titanium present. Figure 1b shows the result of subtracting the interference function of the $(^{48}TiO_2)_{0.18}$-$(SiO_2)_{0.82}$ 750 °C sample from that obtained from the ^{46}Ti-enriched sample; this difference function contains only information about the correlations involving titanium (see eq 2). Structural information is best observed by examining the pair distribution functions obtained by Fourier transformation of the

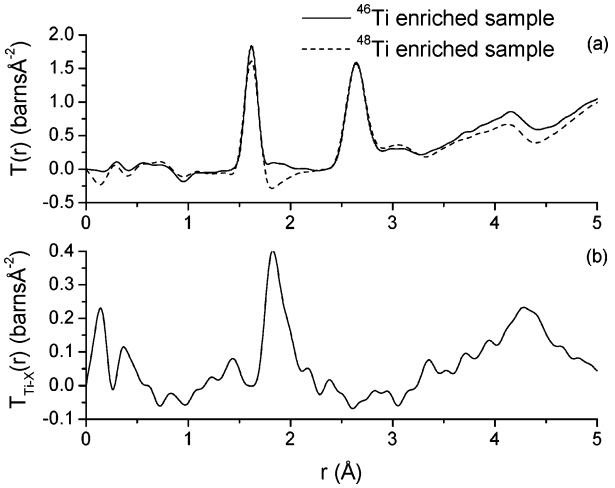

Figure 2. Real-space neutron diffraction data obtained by Fourier transformation of the data shown in Figure 1: (a) total correlation functions, $T(r)$, from the ^{46}Ti-enriched and ^{48}Ti-enriched $(TiO_2)_{0.18}(SiO_2)_{0.82}$ samples heated to 750 °C and (b) difference correlation function showing clearly a feature at just below 2 Å due to Ti−O bonding; the broad feature at ∼4.3 Å is associated with 2nd-neighbor correlations involving Ti (e.g. Ti−O−Si).

Q-space data. Figure 2 shows the real space data obtained by Fourier transformation of the interference functions shown in Figure 1. The two $T(r)$ functions (Figure 2a) are dominated by peaks at ∼1.6 and ∼2.6 Å which are assigned to the Si−O and O−O correlations, respectively. The broader feature at just over 3 Å is due to the Si−Si correlation. The information concerning the Ti−O correlation is contained in the weak features between 1.75 and 2.10 Å and consequently this is the region where the two spectra differ significantly. It is important to note how weak the features in this region are; it is only by taking the difference between the $i(Q)$ functions and obtaining a real space correlation function by Fourier transformation that information about the Ti environment can accurately be obtained. Figure 2b illustrates this point well. The Ti−O correlation clearly contains two distances at ∼1.8 and ∼2.0 Å, with the latter seen as a distinct, partially resolved shoulder. This is the *first* direct, unequivocal observation of two Ti−O distances in this type of material.

The neutron diffraction data were analyzed by using the *Q*-space simulation approach described in the Experimental Section. The structural parameters obtained from simulation of the individual interference functions are presented in Table 2 and those obtained from fitting the difference functions are given in Table 3. Figure 3 serves both as an illustration of the change in the total pair distribution functions as a function of composition and as an example of the quality of the simulations. Figures 4 and 5 show the fits to the real-space difference correlation functions obtained from the $(TiO_2)_{0.08}(SiO_2)_{0.92}$ and $(TiO_2)_{0.18}(SiO_2)_{0.82}$ samples, respectively, and illustrate the structural evolution of the titanium environment as a function of the temperature of heat treatment. Figures 6−8 show the ^{17}O and ^{49}Ti NMR spectra from all three compositions after heat treatment to various temperatures. Peak positions and line widths from the ^{49}Ti NMR spectra are given in Table 4.

The parameters listed in Tables 2 and 3, when combined with the NMR results, give a unique insight into the structural evolution that occurs in this class of materials as a function both of composition and of processing temperature. This structural development (and its implications for materials processing) is discussed in detail below.

$(TiO_2)_{0.08}(SiO_2)_{0.92}$ Samples. The low Ti concentration samples are structurally the least complicated of those studied here. First, we consider the structural evolution of the titanium environment. Examining Figure 4 and Table 3, it may be seen that for the higher processing temperatures only one Ti

TABLE 2: Structural Parameters Obtained from the Simulation of the $T(r)$ Functions from the Isotopically Enriched Samples[a]

sample	correlation	R/Å (±0.01)	N/% (±20)	σ/Å (±0.01)
$(^{46}TiO_2)_{0.08}(SiO_2)_{0.92}$ 250 °C	Si−O	1.61	3.7	0.04
	O−O	2.64	4.3	0.09
	O−O	2.89	0.7	0.09
	Si−Si	3.02	2.6	0.11
$(^{46}TiO_2)_{0.08}(SiO_2)_{0.92}$ 500 °C	Si−O	1.62	4.0	0.04
	O−O	2.64	4.7	0.08
	O−O	2.93	0.5	0.07
	Si−Si	3.03	3.1	0.09
$(^{46}TiO_2)_{0.08}(SiO_2)_{0.92}$ 750 °C	Si−O	1.62	4.2	0.03
	O−O	2.64	5.0	0.08
	O−O	2.82	0.4	0.09
	Si−Si	3.05	3.9	0.09
$(^{46}TiO_2)_{0.18}(SiO_2)_{0.82}$ 250 °C	Si−O	1.61	3.85	0.04
	O−O	2.64	3.95	0.09
	O−O	2.86	0.5	0.08
	Si−Si	3.05	3.8	0.08
$(^{46}TiO_2)_{0.18}(SiO_2)_{0.82}$ 500 °C	Si−O	1.62	4.0	0.04
	O−O	2.64	4.7	0.09
	O−O	2.90	0.7	0.09
	Si−Si	3.04	3.9	0.10
$(^{46}TiO_2)_{0.18}(SiO_2)_{0.82}$ 750 °C	Si−O	1.62	4.0	0.04
	O−O	2.65	4.6	0.08
	O−O	2.90	0.6	0.09
	Si−Si	3.05	4.1	0.09
$(^{48}TiO_2)_{0.41}(SiO_2)_{0.59}$ 250 °C	Si−O	1.61	3.7	0.04
	Ti−O	1.81	1.5	0.06
	Ti−O	1.94	2.7	0.08
	Ti−O	2.10	2.1	0.09
	O−O	2.64	3.7	0.10
	O−O	2.89	1.4	0.09
	Si−Si	3.04	2.5	0.11
$(^{48}TiO_2)_{0.41}(SiO_2)_{0.59}$ 500 °C	Si−O	1.62	4.0	0.04
	Ti−O	1.81	1.4	0.05
	Ti−O	1.95	2.8	0.08
	Ti−O	2.15	0.7	0.09
	O−O	2.64	4.5	0.10
	O−O	2.89	1.5	0.10
	Si−Si	3.03	3.6	0.09

[a] R, N, and σ represent the atomic separation, coordination number, and disorder factor, respectively. σ is derived from the measured peak width and arises from a combination of thermal and static disorder.

TABLE 3: Structural Parameters for the Ti−O Correlations Obtained from the Simulation of the Single Difference Correlation Functions, $T_{Ti-X}(r)$[a]

sample	correlation	R/Å (±0.01)	N/% (±20)	σ/Å (±0.01)
$(TiO_2)_{0.08}(SiO_2)_{0.92}$ 250 °C	Ti−O	1.84	3.3	0.04
	Ti−O	2.01	1.7	0.03
$(TiO_2)_{0.08}(SiO_2)_{0.92}$ 500 °C	Ti−O	1.82	3.7	0.05
$(TiO_2)_{0.08}(SiO_2)_{0.92}$ 750 °C	Ti−O	1.83	3.6	0.04
$(TiO_2)_{0.18}(SiO_2)_{0.82}$ 250 °C	Ti−O	1.89	3.6	0.08
	Ti−O	2.11	1.5	0.05
$(TiO_2)_{0.18}(SiO_2)_{0.82}$ 500 °C	Ti−O	1.84	3.0	0.06
	Ti−O	2.02	1.4	0.06
$(TiO_2)_{0.18}(SiO_2)_{0.82}$ 750 °C	Ti−O	1.81	2.4	0.03
	Ti−O	1.95	1.7	0.06
$(TiO_2)_{0.41}(SiO_2)_{0.59}$ 500 °C	Ti−O	1.82	0.9	0.05
	Ti−O	1.95	2.9	0.11

[a] Each $T_{Ti-X}(r)$ was derived from the difference between the interference functions from the ^{46}Ti- and ^{48}Ti-enriched samples, except that from the $(^{48}TiO_2)_{0.41}(SiO_2)_{0.59}$ composition which was the difference between the data from the ^{nat}Ti- and ^{48}Ti-enriched samples. R, N, and σ represent the atomic separation, coordination number, and disorder factor, respectively.

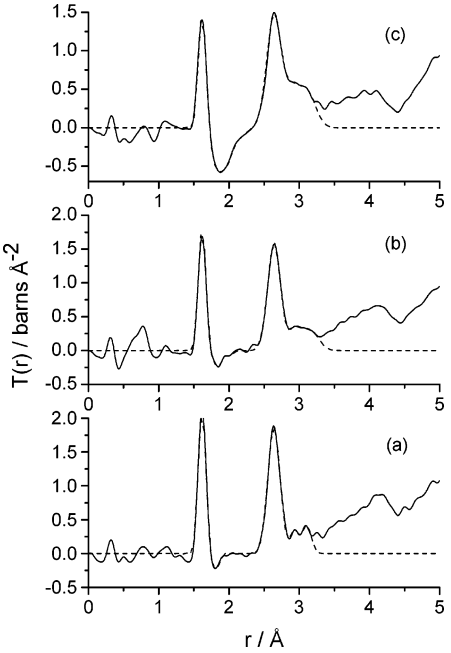

Figure 3. Simulations of the neutron diffraction $T(r)$ functions obtained from the samples heated to 500 °C: (a) $T(r)$ function from the $(TiO_2)_{0.08}(SiO_2)_{0.92}$ sample (solid line) and simulation (dashed line), (b) $T(r)$ function from the $(TiO_2)_{0.18}(SiO_2)_{0.82}$ sample (solid line) and simulation (dashed line), and (c) $T(r)$ function from the $(TiO_2)_{0.41}(SiO_2)_{0.59}$ sample (solid line) and simulation (dashed line).

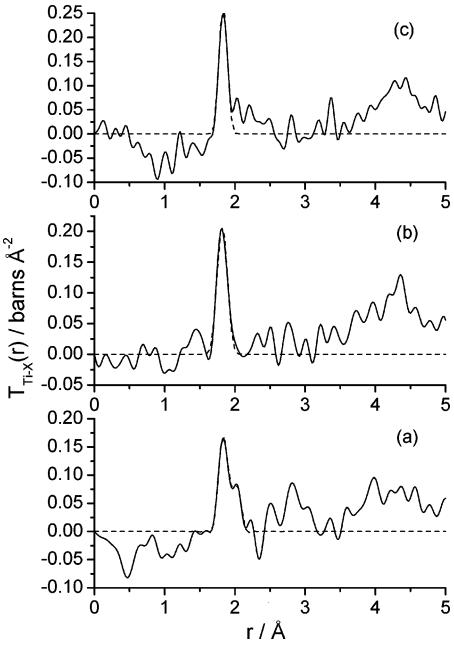

Figure 4. Simulations of the neutron diffraction difference functions, $T_{Ti-X}(r)$, from the $(TiO_2)_{0.08}(SiO_2)_{0.92}$ samples: (a) $T_{Ti-X}(r)$ from the sample heated to 250 °C (solid line) and simulation (dashed line), (b) $T_{Ti-X}(r)$ from the sample heated to 500 °C (solid line) and simulation (dashed line), and (c) $T_{Ti-X}(r)$ from the sample heated to 750 °C (solid line) and simulation (dashed line).

environment is present, which is described by a Ti−O distance of 1.82 Å and coordination number of close to 4.

This Ti−O distance is consistent with all the titanium being tetrahedrally substituted into the silica network.[3] For the sample heated to 250 °C, two Ti−O distances are observed, one at 1.84 Å due to tetrahedrally substituted titanium and a longer distance at 2.01 Å due to six-coordinate titanium.[31] The average Ti−O coordination number of ∼5 also suggests the presence of some

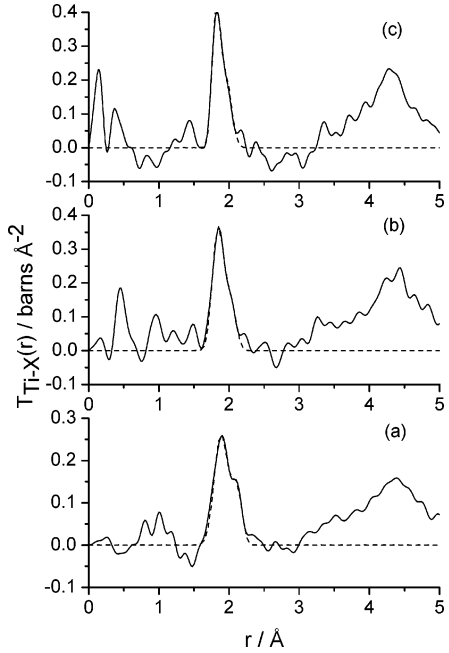

Figure 5. Simulations of the neutron diffraction difference functions, $T_{Ti-X}(r)$, from the $(TiO_2)_{0.18}(SiO_2)_{0.82}$ samples: (a) $T_{Ti-X}(r)$ from the sample heated to 250 °C (solid line) and simulation (dashed line), (b) $T_{Ti-X}(r)$ from the sample heated to 500 °C (solid line) and simulation (dashed line), and (c) $T_{Ti-X}(r)$ from the sample heated to 750 °C (solid line) and simulation (dashed line).

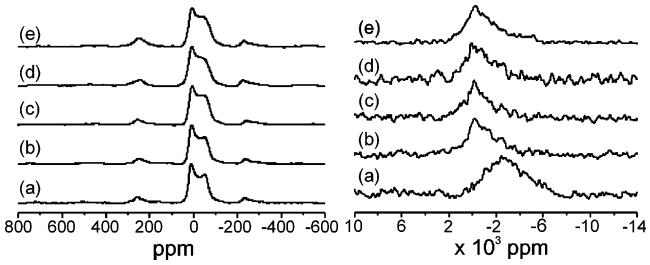

Figure 6. ^{17}O MAS (left) and ^{49}Ti static (right) NMR spectra from the $(TiO_2)_{0.08}(SiO_2)_{0.92}$ samples after various heat treatments: (a) unheated, (b) 120 °C, (c) 250 °C, (d) 500 °C, and (e) 750 °C.

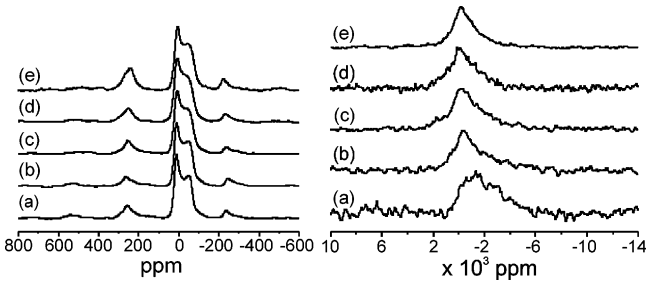

Figure 7. ^{17}O MAS (left) and ^{49}Ti static (right) NMR from the $(TiO_2)_{0.18}(SiO_2)_{0.82}$ samples after various heat treatments: (a) unheated, (b) 120 °C, (c) 250 °C, (d) 500 °C, and (e) 750 °C.

5- or 6-fold titanium. The reason behind this apparent expansion of the titanium coordination sphere in the low-temperature sample in probably due to the strong preference of Ti^{IV} for octahedral coordination combined with the flexibility of the incomplete silica network in which it resides. The additional oxygen ligands are likely to be H_2O and OH^- groups which may be considered as abundant in such a silica network.

The existence of similar titanium sites has previously been inferred on the basis of XANES measurements. Behrens et al.[32] suggested that framework titanium in TS-1 can increase its

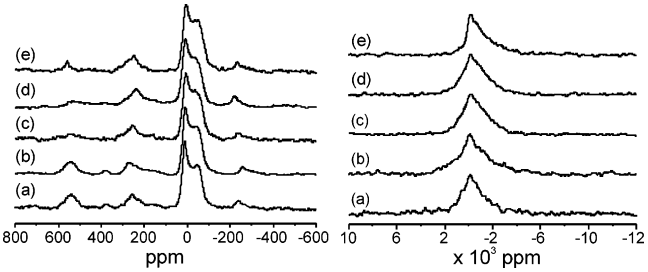

Figure 8. ^{17}O MAS (left) and ^{49}Ti static (right) NMR from the $(TiO_2)_{0.41}(SiO_2)_{0.59}$ samples after various heat treatment: (a) unheated, (b) 120 °C, (c) 250 °C, (d) 500 °C, and (e) 750 °C.

TABLE 4: ^{49}Ti NMR Data for $(TiO_2)_x(SiO_2)_{1-x}$ Sol−Gel Glasses[a]

sample composition	temp/°C	fwhm/ppm	δ/ppm
$(TiO_2)_{0.08}(SiO_2)_{0.92}$	unheated	4425	−2715
	120	2800	−215
	250	2600	−170
	500	2200	−130
	750	2125	−130
$(TiO_2)_{0.18}(SiO_2)_{0.82}$	unheated	3750	−1155
	120	2700	−375
	250	2700	−325
	500	2350	−135
	750	1875	−135
$(TiO_2)_{0.41}(SiO_2)_{0.59}$	unheated	1925	−90
	120	2250	−90
	250	2520	−170
	500	2350	−170
	750	1580	−170

[a] fwhm and δ represent the line width and ^{49}Ti peak position, respectively. Errors: fwhm ±100 ppm, δ ±50 ppm.

coordination from 4- to 6-fold in the presence of H_2O, OH^-, and silanol groups. More recently, in situ high-temperature XANES measurements have been performed on titanium-containing silica sol−gels and the results revealed the existence of TiO_6 sites which could be reversibly converted to TiO_4 sites upon heating to 150−250 °C.[12,13] The results presented here are not only in qualitative agreement with previous measurements but also provide the first direct and accurately quantitative observation of bond distances and coordination numbers associated with these novel TiO_6 sites.

Heating the $(TiO_2)_{0.08}(SiO_2)_{0.92}$ sample to higher temperatures (500 and 750 °C) converts these TiO_6 sites to TiO_4, as demonstrated by the decreasing average bond distance and coordination number shown in Table 3. This change is accompanied by a decrease in the disorder factor, σ, for the Ti−O correlation, which is indicative of the titanium environment becoming less disordered as the temperature of the heat treatment is increased. A better understanding of the structural changes that occur with heat treatment can be gained by considering the silica network in which the titanium atoms are located. Examining the data in Table 2, it can be seen that there is an increase with temperature in both the Si−Si and O−O coordination numbers for the correlations at 3.03 and 2.64 Å, respectively. These changes are consistent with the densification and consolidation of the silica network with temperature through the loss of H_2O, OH^-, and residual organic fragments. Again these changes are accompanied by a decrease in the disorder factors associated with the two correlations, indicating that the overall structure is becoming more ordered as a function of the temperature of the heat treatment. It seems that it is this loss of flexibility in the structure that prevents the TiO_4 groups from increasing their coordination to become TiO_6, as a proportion do in the sample heated to 250 °C.

There is one more correlation in Table 2 that has yet to be discussed, that is, the second O−O distance at ∼2.9 Å. This feature is weak and difficult to assign but its inclusion is necessary to obtain a good simulation of the data and its position is quite consistent between datasets. The most likely origin of this feature is an O−O distance associated with the TiO_x polyhedra. Assuming regular polyhedra and using a Ti−O distance of 1.82 Å for TiO_4 and 2.01 Å for TiO_6, one can calculate O−Ti−O distances of 2.97 and 2.84 Å for tetrahedral and octahedral titanium, respectively. Given the error associated with fitting such a small feature, it would seem that these calculated distances are consistent with the assignment, although it is difficult to draw any meaningful conclusions from the parameters derived from this peak.

The ^{17}O MAS NMR spectra from the $(TiO_2)_{0.08}(SiO_2)_{0.92}$ samples shown in Figure 6 are dominated by the second-order quadrupole line shape at ∼0 ppm that is from Si−O−Si, with some contribution from Si−O−H. The small peak at ∼270 ppm is from Ti−O−Si and there is no Ti−O−Ti signal. The titanium results show broad resonances at all temperatures. There is a very large shift in the unheated gel that is not a chemical shift but from a magnetic contribution that disappears by heating the sample to 250 °C (this has been confirmed by magnetic susceptibility measurements). Although there is significant error on the peak positions given in Table 4 (which, for such a quadrupole nucleus, is not necessarily the isotropic chemical shift), there is a definite trend to more positive values. Also, the line width decreases significantly with heat treatment suggesting, in agreement with the NDIS analysis, that the titanium site is becoming more ordered in this sample as it is heated.

$(TiO_2)_{0.18}(SiO_2)_{0.82}$ Samples. This composition exhibits very interesting structural behavior with significant changes occurring throughout the temperature range studied. It can be seen from Figure 5a that the titanium site in the sample heated to 250 °C is characterized by a very broad correlation due to Ti−O bonding. The results in Table 3 again suggest at least two distinct Ti−O distances. The neutron difference data can be simulated by an average titanium nearest-neighbor environment of four oxygen atoms at a distance of 1.89 Å and two oxygen atoms at a longer distance of 2.11 Å. This type of distorted octahedral environment is observed in the mineral ramsayite, which has four shorter Ti−O bond lengths in the range 1.82−1.96 Å and two in the range 2.14−2.18 Å.[31] As with the $(TiO_2)_{0.08}(SiO_2)_{0.92}$ 250 °C sample, the origin of this distorted TiO_6 site in this sample appears to be the desire of Ti^{IV} to expand its coordination sphere above four by forming longer non-network forming bonds to H_2O and OH^- ligands. In the case of the $(TiO_2)_{0.18}(SiO_2)_{0.82}$ 250 °C samples, this expansion of the titanium coordination sphere from four to six occurs more extensively probably due to the higher concentration of the metal, which allows it to exert a greater influence over the structure as a whole. Further evidence that the longer Ti−O distances are indeed due to weaker bonds to H_2O and OH^- ligands comes from a previous high-temperature XANES study[12] that demonstrated the abundance of reversible $TiO_6 \leftrightarrow TiO_4$ sites in the structure of samples of this composition.

After the sample is heated to 750 °C, the titanium environment in the $(TiO_2)_{0.18}(SiO_2)_{0.82}$ sample becomes more well-defined as can be witnessed by the much narrower Ti−O correlation in Figure 5c. The parameters derived from the simulation analysis of this feature given in Table 3 indicate that two Ti−O distances are present, a short distance at 1.81 Å due to titanium tetrahedrally substituted within the silica network

and a longer distance at 1.95 Å, which is very close to the average Ti−O bond length determined from the mineral anatase (one of the crystalline forms of TiO_2 that has a structure consisting of TiO_6 octahedra).[33] The average Ti−O coordination number determined at this temperature of heat treatment is close to four, suggesting that the majority of titanium in this sample is substituted within the silica network with a minority species present in a TiO_6 environment similar to that found in anatase. Indeed, the $(TiO_2)_{0.18}(SiO_2)_{0.82}$ 750 °C sample containing natural titanium exhibited very weak Bragg peaks in the $i(Q)$ data, the positions of which corresponded to those expected for anatase. Hence, it seems that at least some of the TiO_6 present in the samples heated to 750 °C is in the form of phase-separated TiO_2, which is on the point of crystallization at this temperature.

At the intermediate temperature of heat treatment, the Ti−O environment in the $(TiO_2)_{0.18}(SiO_2)_{0.82}$ sample is very similar to that found in the $(TiO_2)_{0.08}(SiO_2)_{0.92}$ sample heated to 250 °C. The results in Table 3 are consistent with a mixed environment of TiO_4 sites and unstable, distorted TiO_6 sites. One difference between the results obtained from the $(TiO_2)_{0.18}(SiO_2)_{0.82}$ 500 °C sample and those from the $(TiO_2)_{0.08}(SiO_2)_{0.92}$ 250 °C sample is that the disorder factors for the Ti−O correlations are significantly larger in the former, suggesting greater disorder in the structure of the Ti−O sites. This disorder may be associated with the presence of nonisolated TiO_6, which leads to a small amount of phase separation of TiO_2 when the sample is heated to higher temperature. There is an overall decrease in average Ti−O coordination number and associated decrease in the average Ti−O distance as the temperature of the heat treatment is increased. These changes are consistent with the conversion of TiO_4 sites to TiO_6 sites as a function of temperature and agree well with the results of previous structural studies with XRD, and ^{29}Si MAS NMR, XANES, and EXAFS.[11,34,35]

The results in Table 2 yield information on the behavior of the silica network in the $(TiO_2)_{0.18}(SiO_2)_{0.82}$ samples as a function of the temperature of the heat treatment. Similar trends are observed to those witnessed with the $(TiO_2)_{0.08}(SiO_2)_{0.92}$ samples, with both the Si−Si and O−O nearest-neighbor coordination numbers increasing with temperature due to the densification and consolidation of the silica network. Once more a correlation is observed at ∼2.9 Å, which is assigned to the O−O distance in the TiO_x polyhedra, although no reliable structural information can be determined from this feature.

The ^{17}O NMR MAS spectra in Figure 7 again show a strong signal from the second-order quadrupole line shape at ∼0 ppm from Si−O−Si, and the Ti−O−Si peak at ∼270 ppm is significantly stronger than that for the $(TiO_2)_{0.08}(SiO_2)_{0.92}$ sample, simply reflecting the higher titanium content of this sample, and hence increase in Ti−O−Si bonding. In this sample there is now a small but nevertheless distinct peak at ∼550 ppm corresponding to Ti−O−Ti, probably as OTi_3.[18] Again titanium shows broad resonances at all temperatures with an unexpectedly large shift in the unheated gel, although it is not as large as that for the $(TiO_2)_{0.08}(SiO_2)_{0.92}$ xerogel. The source of this is again a magnetic susceptibility contribution that is lost on heating the sample to 250 °C. The peak shows the same trend to more positive values, and a significant decrease in line width, with heat treatment (Table 4) again suggesting that the titanium site is becoming more ordered. The sensitivity of the titanium, even when enriched in ^{49}Ti, does not allow unambiguous detection of a distinct TiO_6 site. It is use of ^{17}O NMR that helps to unequivocally show that a very small amount of phase separation is occurring. As well as agreeing with the results from the NDIS analysis, these NMR results confirm that the $(TiO_2)_{0.18}(SiO_2)_{0.82}$ composition is indeed on the limit of solubility of TiO_2 in sol−gel silica.[11, 24]

$(TiO_2)_{0.41}(SiO_2)_{0.59}$ Samples. Due to the high concentration of titanium in these samples and the cost of the ^{46}Ti isotope there is a more limited set of neutron difference data collected at this composition. This problem was compounded by the fact that, due to the high metal content, some of the samples displayed evidence of significant levels of crystallization after being heated to only 250 °C. As can be seen from Table 3, only the difference between the data from the ^{nat}Ti- and ^{48}Ti-enriched samples heated to 500 °C is included. The relatively small difference in neutron scattering lengths between ^{nat}Ti ($b = -3.438$ fm) and ^{48}Ti ($b = -6.063$ fm) means that the features in the $T_{Ti-X}(r)$ function are weak compared to those shown in Figures 4 and 5. However, the strong scattering properties of ^{48}Ti and its high concentration in these samples partially mitigate these limitations by allowing reliable information concerning the titanium environment to be determined from the ^{48}Ti $i(Q)$ functions. The difference function from the 500 °C samples augments this information and assists in the assignment of the correlations involving titanium.

The results in Table 2 suggest that there are three distinct Ti−O distances present at both temperatures of heat treatment. The short Ti−O distance at 1.81 Å can again be assigned to titanium substituted tetrahedrally within the silica network, the middle distance at 1.95 Å is due to TiO_6 sites similar to those found in anatase, and the long distance of 2.10−2.15 Å is associated with titanium atoms that have expanded their coordination sphere from four coordinate to six coordinate by bonding to H_2O and OH^- ligands. Consistent with previous structural studies,[7,8,34] the presence of the distance at 1.95 Å is evidence of phase separation of TiO_2 at this composition. Both samples exhibit a Ti−O coordination number of ∼1.5 for the correlation at 1.81 Å and ∼2.8 for the correlation at 1.95 Å. Assuming a reasonable uncertainty of ±20% in these coordination numbers, it can be calculated that around 60(±10)% of the titanium is present as phase-separated TiO_2. The remaining 40% must be present as isolated TiO_4 and TiO_6 groups; this amounts to 16 mol % of the total 41 mol %, suggesting that, in agreement with the results from the $(TiO_2)_{0.18}(SiO_2)_{0.82}$ samples and those of previous studies,[11,24] the solubility limit of TiO_2 in sol−gel prepared silica is in the range of 11 to 16 mol %.

Considering the structural evolution that occurs within the $(TiO_2)_{0.41}(SiO_2)_{0.59}$ samples as a function of temperature, it is seen that the coordination number for the correlation at ∼2.1 Å drops from over two to below one as the temperature of the heat treatment is raised from 250 to 500 °C. The reason for this is the loss of H_2O and OH^- ligands from the network as densification of the sol−gel structure takes place. Supporting evidence for this explanation comes from the accompanying increase in the Si−Si and O−O nearest neighbor coordination numbers. It seems from the coordination numbers in Table 2 that there is no significant increase in the fraction of phase-separated titanium after heating to 500 °C. However, careful examination of the difference data in Q-space reveals the presence of weak Bragg peaks due to anatase at this temperature of heat treatment. These results suggest that the onset of crystallization of the phase-separated TiO_2 is at a lower temperature for the $(TiO_2)_{0.41}(SiO_2)_{0.59}$ composition than for the $(TiO_2)_{0.18}(SiO_2)_{0.82}$ composition. This difference is possibly due to the difference in size of the phase-separated TiO_2 domains, which may have an effect on the kinetics of the nucleation process.

The ^{17}O NMR MAS spectra in Figure 8 again show a strong signal from the second-order quadrupole line shape at ~0 ppm from Si−O−Si. The secondary peaks are the Ti−O−Si peak at ~270 ppm and a peak at ~550 ppm, probably from Ti−O−Ti. Their intensities relative to the Si−O−Si resonance provide much useful information about the structure. The Ti−O−Si resonance is about the same relative intensity as that for the $(TiO_2)_{0.18}(SiO_2)_{0.82}$ sample. This indicates that the amount of Ti−O−Si bonding is similar between these samples agreeing with the estimate from the neutron data of the TiO_2 content within the silica network. The higher titanium content is reflected in a more intense Ti−O−Ti line, indicating that more phase separation has occurred in this sample. It is also interesting to note that in the sample heated to 750 °C the Ti−O−Ti resonance sharpens, indicating that crystallization of TiO_2 is occurring. The titanium NMR shows some interesting contrasts to that from the other two samples. Notably the shift is of a value more typical of that from a diamagnetic material at all temperatures of heat treatment. Also, although the line shape has the broad asymmetric component similar to the lower TiO_2-content samples, there is a distinct, sharp component (although not resolved) that is at a very similar shift to the ^{49}Ti peak in anatase. The NMR is in a high degree of agreement the other measurements in that the indication is that there is still significant titanium bonding to the silicon, but that phase separation also occurs as TiO_2.

Of the solid-state titanium NMR reported to date[18,21] relatively little has been from compounds containing Ti−O−Si bonding. In $CaTiSiO_5(TiO_6)$, $Na_2TiSiO_5(TiO_5)$, and $Li_2TiSiO_5(TiO_5)$ the quadrupole coupling constant is in the range 13.2 to 18.2 MHz.[21] In these materials a distinct second-order quadrupole line shape could be discerned, which could be simulated to deduce the isotropic chemical shift. This chemical shift differed between TiO_6 and TiO_5 by ~100 ppm. Once the different second-order quadrupole effects are accounted for[36] the peak position alone is probably discriminatory enough to distinguish between the different species as the peak ranges overlap. There are only very small differences in the titanium peak positions in these samples so they do not provide unequivocal evidence of the nature of the titanium site. It is also interesting to compare these results with those recently reported on titanium substitution in zeolite USY.[37] A relatively narrow titanium resonance (fwhm ~500 ppm) at ca. −90 ppm (on our shift reference scale) was detected and assigned to TiO_6 substituting into the silica-dominated framework. Hence there do appear to be a large range of parameters associated with titanium in a silicate-type environment and it will be a significant challenge to determine both the interaction parameters accurately and relate them to structural detail to which they appear very sensitive.

There are some general comments that can be made about the processing of these materials from the trends observed in the results presented here. First, examining the structural changes that occur in the $(TiO_2)_{0.08}(SiO_2)_{0.92}$ and $(TiO_2)_{0.18}(SiO_2)_{0.82}$ samples as a function of temperature of the heat treatment applied, it is evident that the most significant structural changes involving the titanium environment occur between 250 and 500 °C; heating to 750 °C has only a small effect on the titanium environment with the main structural evolution involving the densification and consolidation of the silica network. This point has important implications in the area of catalysis where both the nature of the titanium site and overall surface area of the sample are important.[4,5] In fact, a study by the authors of the performance of $(TiO_2)_{0.18}(SiO_2)_{0.82}$ sol−gel catalysts toward the epoxidation of cyclohexane revealed that the most active sample was one calcined at 500 °C whereas heating to 750 °C resulted in a marked drop in turnover.[27] The second point to note is that the quantitative results from this study agree fully with the results of the Ti K-edge XANES studies performed by the authors on similar TiO_2-SiO_2 sol−gel materials.[11,12] The importance of this is it illustrates how valuable the qualitative XANES technique is when examining the titanium environment on such materials.

Conclusions

Neutron diffraction with isotopic substitution combined with ^{17}O and ^{49}Ti solid-state NMR have unequivocally established the behavior of TiO_2 in sol−gel prepared silica at an atomic level over a wide range of compositions.

The results from the $(TiO_2)_{0.08}(SiO_2)_{0.92}$ samples show that after they have been heated to over 500 °C all of the titanium can be considered as substituted for silicon in a tetrahedral environment within the glass network. As expected, this environment has a Ti−O bond distance of 1.82 Å. After heating at the lower temperature of 250 °C, two titanium environments are present: one tetrahedral within the network and one octahedral within the network where the titanium has expanded its coordination sphere to six by bonding to H_2O and OH^- ligands. The ^{17}O results, which are particularly sensitive to phase separation at the level of enrichment used in this study, show no evidence of phase separation at this composition.

The $(TiO_2)_{0.18}(SiO_2)_{0.82}$ samples exhibit the presence two titanium environments at low temperature, the tetrahedrally substituted site and the distorted octahedral site created when the titanium forms two extra bonds to H_2O and OH^- ligands. Heating the sample to higher temperature converts some of the distorted octahedral sites to tetrahedral sites while the remainder becomes less distorted and more similar to the titanium site in anatase. A small amount of phase separation of TiO_2 is confirmed by both the neutron diffraction and the ^{17}O MAS NMR. These results confirm that this composition is indeed on the limit of solubility of TiO_2 in sol−gel derived silica.

As expected, the $(TiO_2)_{0.41}(SiO_2)_{0.59}$ samples exhibit the presence of phase separation of TiO_2 at all temperatures of heat treatment. Both the neutron diffraction and ^{17}O MAS NMR results suggest that the level of TiO_2 that can be considered as dissolved in the silica network is the same at this composition as in the $(TiO_2)_{0.18}(SiO_2)_{0.82}$ samples. In agreement with previous studies,[11,24] the results presented here suggest that the limit of solubility of TiO_2 in sol−gel derived silica is in the region of 15 mol %.

Acknowledgment. The EPSRC are thanked for funding the collaboration between Kent and Warwick on sol−gel materials, K.O.D. thanks the EPSRC and the ESRF for a studentship and M.E.S. thanks the EPSRC, HEFCE and the University of Warwick for the funding of the NMR equipment.

References and Notes

(1) Brinker, C. J.; Scherer, G. W. *Sol−Gel Science*: *The Physics and Chemistry of Sol−Gel Processing*; Academic: San Diego, CA, 1990.

(2) Schultz, P. C.; Smyth, H. T. In *Amorphous Materials*; Douglas, R. W., Ellis, B., Eds.; Wiley: London, UK, 1970; p 453.

(3) Davis, R. J.; Liu, Z. *Chem. Mater.* **1997**, *9*, 2311−2324.

(4) Imamura, S.; Nakai, T.; Kanai, H.; Ito, T. *J. Chem. Soc., Faraday Trans.* **1995**, *91*, 1261−1266.

(5) Beck, C.; Mallat, T.; Bürgi, T.; Baiker, A. *J. Catal.* **2001**, *204*, 428−439.

(6) Walther, K. L.; Wokaun, A.; Handy, B. E.; Baiker, A. *J. Non-Cryst. Solids* **1991**, *134*, 47−57.

(7) Dirken, P. J.; Smith, M. E.; Whitfield, H. J. *J. Phys. Chem.* **1995**, *99*, 395−401.

(8) Anderson, R.; Mountjoy, G.; Smith, M. E.; Newport, R. J. *J. Non-Cryst. Solids* **1998**, *234*, 72−79.

(9) Rigden, J. S.; Walters, J. K.; Dirken, P. J.; Smith, M. E.; Bushnell-Wye, G.; Howells, W. S.; Newport; R. J. *J. Phys.*: *Condens. Matter* **1997**, *9*, 4001−4016.

(10) Farges, F.; Brown, G. E.; Rehr, J. J. *Phys. Rev. B* **1997**, *56*, 1809−1819.

(11) Mountjoy, G.; Pickup, D. M.; Wallidge, G. W.; Anderson, R.; Cole, J. M.; Newport, R. J.; Smith, M. E. *Chem. Mater.* **1999**, *11*, 1253−1258.

(12) Mountjoy, G.; Pickup, D. M.; Wallidge, G. W.; Cole, J. M.; Newport, R. J.; Smith, M. E. *Chem. Phys. Lett.* **1999**, *304*, 150−154.

(13) Grunwaldt, J.-D.; Beck, C.; Stark, W.; Hagen, A.; Baiker, A. *Phys. Chem. Chem. Phys.* **2002**, *4*, 3514−3521

(14) Gaskell, P. H. In *Materials Science and Technology*; Zrzycky, J., Ed.; VCH: Weinhaim, Germany, 1991; Vol. 9, pp 175−278.

(15) Wada, M.; Kamiya, K.; Nasu, H.; Matsuoka, J.; Yoko, T.; Fukunaga, T.; Misawa, M. *J. Non-Cryst. Solids* **1992**, *149*, 203−208.

(16) Brequel, H.; Enzo, S.; Babonneau, F.; Radaelli, P. G. *Mater. Sci. Forum* **2002**, *386*, 275−280.

(17) Cormier, L.; Gaskell, P. H.; Calas, G.; Soper, A. K. *Phys. Rev. B* **1998**, *58*, 11322−11330.

(18) MacKenzie, K. J. D.; Smith, M. E. *Multinuclear Solid State NMR of Inorganic Materials*; Pergamon Press: Oxford, UK, 2002.

(19) Gunawidjaja, P. N.; Holland, M. A.; Mountjoy, G.; Pickup, D. M.; Newport, R. J.; Smith, M. E. *Solid State NMR* **2003**, *23*, 88−106.

(20) Gervais, C.; Babonneau, F.; Smith, M. E. *J. Phys. Chem. B* **2001,** *105*, 1971−1977.

(21) Padro, D.; Jennings, V.; Smith, M. E.; Hoppe, R.; Thomas, P. A.; Dupree, R.; *J. Phys. Chem. B* **2002**, *106*, 13176−13185.

(22) Bastow, T. J.; Whitfield, H. J. *Chem. Mater.* **1999**, *11*, 3518−3520.

(23) Gervais, C.; Smith, M. E.; Pottier, A.; Jolivet, J.-P.; Babonneau, F. *Chem. Mater.* **2001**, *13*, 462−467.

(24) Evans, D. L. *J. Non-Cryst. Solids* **1982**, *52*, 115−128.

(25) Barksdale, J. *Titanium*; Ronald Press: New York, 1966.

(26) Tsvetkov, V. F.; Likhomanenko, V. A.; Pisareva, V. S.; Korzhova, N. V.; Kazantsez, V. M.; Korshunov, S. P.; Zakharkin, L. I. *J. Appl. Chem. USSR (Engl. Transl.)* **1983**, *56*, 1036−1039.

(27) Holland, M. A.; Pickup, D. M.; Mountjoy, G.; Tsang, S. C. E.; Wallidge, G. W.; Smith, M. E.; Newport, R. J. *J. Mater. Chem.* **2000**, *10*, 2495−2501.

(28) Hannon, A. C.; Howells, W. S.; Soper, A. K. In *Proceedings of the Second Workshop on Neutron Scattering Data Analysis*; IOP Conference Series No. 107; Johnson, M. W., Ed.; Institute of Physics: Bristol, UK, 1990; p 193.

(29) Yarker, C. A.; Johnson, P. A. V.; Wright, A. C.; Wong, J.; Greegor, R. B.; Lytle, F. W.; Sinclair, R. N. *J. Non-Cryst. Solids* **1986**, *79*, 117−136.

(30) Kunwar, A. C.; Turner, G. L.; Oldfield, E. *J. Magn. Reson.* **1986**, *69*, 124−127.

(31) The United Kingdom Chemical Database Service: Fletcher, D. A.; McMeeking, R. F.; Parkin, D. J. *Chem. Inf. Comput. Sci.* **1996**, *36*, 746−749.

(32) Behrens, P.; Felsche, J.; Vetter, S.; Schulz-Ekloff, G.; Jaeger, N. I.; Niemann, W. *J. Chem. Soc., Chem. Commun.* **1991**, 678−680.

(33) Burdett, J. K.; Hughbanks, T.; Miller, G. J.; Richardson, J. W.; Smith, J. V. *J. Am. Chem. Soc.* **1987**, *109*, 3639−3646.

(34) Pickup, D. M.; Mountjoy, G.; Wallidge, G. W.; Anderson, R.; Cole, J. M.; Newport, R. J.; Smith, M. E. *J. Mater. Chem.* **1999**, *9*, 1299−1305.

(35) Pickup, D. M.; Mountjoy, G.; Roberts, M. R.; Wallidge, G. W.; Newport, R. J.; Smith, M. E. *J. Phys.*: *Condens. Matter* **2000**, *12*, 3521−3529.

(36) Smith, M. E.; van Eck, E. R. H. *Prog. NMR Spectrosc.* **1999**, *34*, 159−201.

(37) Ganapathy, S.; Gore, K. U.; Kumar, R.; Amoureux, J.-P. *Solid State NMR* **2003**, *24*, 184−195.